Effects of Chloride ions on Carbonation Rate of Hardened Cement Paste by X-ray CT Techniques

Jun-zhe Liu[1], Ming-fang Ba[1,2*], Yin-gang Du[2], Zhi-min He [1], Jian-bin Chen[1]

[1]Faculty of Architectural Civil Engineering and Environment, Ningbo University, Ningbo, 315211, China

[2] Faculty of Science and Technology, Anglia Ruskin University, Chelmsford, CM1 1SQ, UK

[*]Corresponding author, Email: bmf-1@163.com

Contact address: Faculty of Architectural Civil Engineering and Environment, Ningbo University, Ningbo 3152 11, China

Abstract: Corrosion of steel bars in concrete structures is initiated as a result of concrete carbonation and/or chloride intrusion, and influenced by their interaction. This paper presents an experimental investigation into the effect of chloride ions on carbonation of cement paste by means of X-ray CT techniques and mercury intrusion porosimetry(MIP), which is benchmarked by the conventional phenolphthalein method. A group of the cement paste cylinders with different amounts of chlorides ions were manufactured and cured before they were subjected to an accelerated carbonation process in a conditional cabinet regime for different ages. The carbonation front of the cement paste was first evaluated using phenolphthalein method. This was followed by an investigation of microstructure evolution of the cement paste using XCT and MIP techniques. The experimental results show that the carbonation of a cement paste increases with its water to cement ratio and with carbonation ages, but decrease with its amount of chloride ions. In particular, it has been found that increases of chloride ion of a cement paste refine its porous structures, decrease its porosity and eventually mitigate its carbonation rate. The relevant results can be referred to for durability design and prediction of reinforced concrete structures.

Key words: cement paste; chloride ions; accelerated carbonation; X-CT; gray values

1. Introduction

Steel corrosion is one of the principal reasons for the deterioration and durability failure of concrete structures. It reduces the effective area of a steel bar in concrete irregularly and decreases its strength and ductility significantly. It causes the cracking of concrete cover due to expansion of corrosion products and hence decreases the stiffness of a structure. It also deteriorates the bond between a corroding bar and its surrounding concrete and therefore alters the behavior of a structure. As a result, the bearing capacity and safety margin of a structure with corroding steel bars decreases substantially. Its anticipated ductile failure mode may be changed into a brittle one without an obvious warning [1-3].

It is well known that steel corrosion is initiated as a result of concrete carbonation and chloride migration [4-10]. Ove the past decades, a significant number of researches have been done on the properties of concrete that is affected either by concrete carbonation or chloride diffusion, respectively [11-13]. Actually, however, most of reinforced concrete structures may suffer from concrete carbonation and chloride intrusion simultaneously with a potential interaction between concrete carbonation and chloride migration.

It has been reported that a penetration of carbon dioxide (CO_2) into a concrete not only causes concrete carbonation and deteriorates concrete structures, but also reduces the capacity of chloride binding and makes more chloride ions released in the pore solution of a carbonated concrete. In addition, the presence of CO_2 results in concrete shrinkage, which in turn promotes the transportation of more external chloride ions into the concrete. As a result, both concentration of chloride ions in the pore solution of the carbonated concrete and the risk of chloride – induced corrosion of steel bars in the concrete increase significantly [14-17]. On other hand, chlorides ions in a concrete reacts chemically with its tricalcium aluminate (C_3A) of a concrete and produces Friedel salt ($3CaO{\cdot}Al_2O_3{\cdot}CaCl_2{\cdot}10H_2O$) during hydration process of the concrete, which in turn increases the pH value of pore solution of a concrete and mitigates the risk of carbonation–induced corrosion of steel bar in the concrete [18].

The above valuable researches do reveal the effect of concrete carbonation on intrusion/concentration of chloride icon in a concrete. However, less significant research has been reported on the effect of chloride intrusion on carbonation of concrete or cement paste. In addition, the carbonation of a concrete is conventionally identified using phenolphthalein method. This method, however, calls for breaking off specimens and does not estimate the carbonation rate in terms of percentage of Portlandites consumption. Actually it is known that carbonation is a gradual phenomenon, partial carbonation after the front determined by means of pulverizing phenolphthalein is not possible [19-23]. Fortunately, both X-ray computed tomography (XCT) and mercury intrusion porosimetry (MIP) facilitate a powerful technology that can accurately image the internal structures of composite and heterogeneous materials in three-dimensions [24-25].

Hence, this paper presents an experimental investigation into the effect of chloride ions on carbonation of cement paste by means of X-ray CT techniques and mercury intrusion porosimetry(MIP), which is benchmarked by the conventional phenolphthalein method. A group of the cement cylinders with different amounts of chlorides ions were manufactured and cured before they were subjected to an accelerated carbonation process in a conditional cabinet regime for different ages. The carbonation front of the cement paste was first evaluated using phenolphthalein spraying method. This was followed by an investigation of microstructure evolution of the cement paste due to carbonation using XCT and MIP techniques, which is vital to transport of carbon dioxide, water, chloride ion and eventually concrete durability [26]. The relevant results can be referred to for durability design and prediction of reinforced concrete structures.

2. Experimental

2.1 Materials and Specimens

An Ordinary Portland cement PO425 in conformity with Chinese Cement standards (GB 175-2007) was used for the manufacturing of the cement paste cylinder specimens with a diameter of 36mm and a height of 100mm. The

cylinder specimens have the water to cement ratios of 0.3, 0.4 and 0.5 and the chloride ions (NaCl) of 0.0%, 0.3%, 0.6% and 1.0% of cement mass, respectively. Following casting of cement mortar, the cylinder specimens were first cured in the standard conditional regime of 20±1°C and 90% relatively humidity for 24 hours, before they were de-molded, wrapped up with plastic film and cured in the same regime for 28 days. At the end of cure period, both top and bottom circular surfaces of each cylinder specimen were sealed with an epoxy. Afterwards, the cylinder specimens were stored in an conditional cabinet for 7 days, 14 days, 21 days and 28 days, respectively, with their side surface exposed to a carbonation regime that has a 20% carbon dioxide (CO_2) in volume and 60% relatively humidity for an accelerated carbonation process.

2.2 Testing methods

2.2.1 Evaluation of carbonation depth using Phenolphthalein method

The carbonation depths of cement paste cylinder specimen were first measured using the conventional method of Phenolphthalein solution, which was adopted to consolidate the results measure by X-CT, as described below. Some cylinder specimens were removed from the conditional cabinet at different carbonation periods, before they were cut into two using a metal saw and the 1% Phenolphthalein alcohol solution was sprayed on one cut surface of the specimen to observe the variation of the surface color and determine the carbonation depth. Another cut surface of the specimen was sealed with epoxy and the remaining part of the specimen was re-conditioned in the cabinet to continue its carbonation process.

2.2.2 Evaluation of carbonation using X-ray CT

Further to the above measurement of carbonation front of all the cement cylinder specimens using Phenolphthalein method, the cement cylinder specimens with water to cement ratios of 0.3 and 0.5 were selected for the investigation of their microstructures evolution at different carbonation age using X-CT technique and analyzed with software named VG Studio MAX 2.1. As illustrated in Fig.1 for its principle, the cement cylinder specimen

was set in a holder that was mounted on a precision rotation table, and then the table position was adjusted to fit the image within the field view. During scanning process, a conical X-ray beam was emitted as the specimen rotates through 360 degree. The X-ray CT raw data were then collected using 1080 projection images that were recorded by a CCD camera with an array of 1024×1024 pixels. As a result, the 3D voxel size was 0.086 mm × 0.086 mm× 0.086 mm [27-28].

2.2.3 Evaluation using mercury intrusion porosimetry (MIP)

By 28-day curing, one of the specimens with different water-to-cement ratios was taken out to prepare samples for MIP testing. To be specified, a hammer was used to slightly rap the specimen and take one small 10-mm pieces (average diameter) with nearly perfect surface for MIP testing.

3. Results and Discussions

3.1 Effect of chloride ions on carbonation of cement paste

3.1.1 Measured carbonation depth using phenolphthalein

Table 1 summaries the carbonation depths of cement cylinder specimens with different water to cement ratios and different chloride ions at different carbonation ages. It is clear that carbonation depth of cement cylinder increases with an increase of carbonation age and an increase of water-to-cement ratio, respectively. For example, for the same amount of 1.0% chloride ions, the carbonation depth of the cement cylinder with a water to cement ratio of 0.3 after 7 days carbonation is 1.90mm, which is much smaller than that of 10.8 mm of the cylinder with water to cement ratio of 0.5 after 28 days carbonation. This is attributed to the fact that a large water to cement ratio increases porosity of cement paste, which prompts the diffusion of carbon dioxide and therefore increases the carbonation depth. The longer the carbonation time, the further the carbon dioxide can move into the cement cylinder and hence increase its carbonation depth. In particular, the results in Table 1 show that an increase of chloride-ions contents in cement paste decreases the corresponding carbonation depth significantly. For the same

water to cement ratio of 0.4 and the same carbonation period of 14 days, the carbonation depth of cement cylinder with 0.3% chloride ions is 7.0mm, which is reduced to 5.9 mm for the cement cylinder with 1.0% chloride ions.

3.1.2 Carbonation results by X-CT testing

The carbonation depths measured using the above phenolphthalein is valuable. However, they are only for the individual destructed section of a cement cylinder, and cannot easily be used to show the overall profile of carbonation of the nondestructive cylinder. In order to more visually observe the carbonation process of specimen, a three-dimensional reconstruction of the tested cylinder and the gray value gradation of each section were obtained by X-CT analytical technique.

Fig.2 and Fig.3 show the three-dimensional reconstruction images and the gray value gradation of the cement cylinders with the chloride ions of 0.3%, 0.6% and 1.0%, the carbonation ages of 0, 7 and 21 days and the water to cement ratios of 0.3 and 0.5, respectively.

It is obvious that either an increase of carbonation ages from 0 to 21 days or a decrease of chloride ions from 1.0% to 0.3% does decrease the diameter and volume of the remaining un-carbonated cement paste, and therefore increases the carbonation depth of cement cylinder. In addition, a comparison of the images between Fig. 2 and Fig. 3 indicates that an increase of water to cement ratio from 0.3 to 0.5 also decreases the diameter and volume of the remaining un-carbonated cement paste, and therefore decreases the carbonation depth of cement cylinder. These observations from X-CT results are clearly consistent with the previous discussions based on the phenolphthalein results in Table 1.

In particular, both Fig 2 and Fig 3 show that the diameters and volumes of the remaining un-carbonated cement paste of lower part of each cylinder specimen is greater than those of upper part of the cylinder. In other words, for the same cement cylinder under the same carbonation regime, the carbonation depth of its upper cement paste is larger than those of its lower part, which is attributed to the fact that, during the manufacturing of cylinder

specimen, the compaction of liquid cement drove the spare water upwards and therefore the water-to-cement ratio of the upper cement is a little bit higher than that of lower cement of the same cement cylinder due to gravity stratification. It is clear that the late observation cannot be easily made using the phenolphthalein method.

In addition to the above qualitative observation, the X-CT techniques also creates the quantitative results in the term of gray values, as shown in Fig 4 and Fig 5 for the specimen with water to cement ratio of 0.5, the chloride ions of 0.3% and 1.0%, and the carbonation ages of 0, 7 and 21 days, respectively. Here, the gray values represent absorption rates and attenuation coefficients at the corresponding object position. The gray values are proportional to the X-ray attenuation coefficient that is strongly correlated with the density of the specimens.

Fig.4 shows that, before carbonation with 0 day of carbonation age, the gray value is about 380 at its peak amount of volume elements, which decreases to about 350 for the carbonated cement cylinders. In addition, the amounts of peak volume elements of the cement cylinders with 0.3% chloride ions decrease steadily from 1100 to 600 as carbonation age increases from 0 to 21 days. For the non-carbonated cement cylinders, an increase of chloride ions from 0.3% to 1.0% decreases the amounts of peak volume elements from 1100 to 900. However, for the carbonated cement cylinder, the effect of chloride ions on the amount of peak volume elements become less significant with the similar values of about 900 for 7 days carnation. This indicates that as carbonation progresses, the density of carbonated products increases and the amounts of peak volume elements corresponding gray values of carbonated products becomes less than those of the non-carbonated parts.

Fig.5 shows a two dimensional (2D) plan view (left), side view (right side) and gray value distribution of a cement cylinder with 0.5 water to cement ratio, 0.3% chloride ion and 0, 7 and 21 days carbonation ages. According to the brightness of the 2D slice, light area is the carbonated cement and dark area is the non-carbonated ones. It is clear that the carbonation front is gradual segment. The gray vale at the point P was dipped in Fig.5, whose corresponding scanning line position referred to pore in the hardened paste. It can be seen that before carbonation

the gray values varies along the diameter of 36mm of cement cylinder varies gently. However, after the 7 and 21 days of carbonation, the gray value changes sharply, especially near the boundaries between the carbonated and non-carbonated zones of cement cylinder. The dotted line in scanning gravy value curve represented the corresponding carbonation front.

3.2 Effects of chloride ions on porous characteristics of non-carbonated cement

By means of mercury intrusion porosimetry (MIP) techniques, the effect of chloride ions on the porous size distribution and accumulated porosity of the non-carbonated cement paste with water to cement ratios of 0.3 and 0.5 are shown in Fig. 6 and 7, respectively, and summarized in Table 2. Before the dissuasion of the MIP results, however, It should be pointed out here that much smaller pores need much higher mercury intrusion force, and thus the corresponding pores with diameter equal or less 5 nm could not be detected precisely[29].

Fig. 6 (a) and Fig. 7(a) show that the cumulative pore volumes of all the cement pastes decrease sharply as their porous diameter increases. In other words, the diameter of the most pores in a cement paste is less than 10 nm. Furthermore, the cumulative pores volumes of all the cement paste with 1.0% chloride ions is always less than those of the cement paste without chloride ions. A comparison of Fig. 6(a) and Fig. 7(a) also shows that the cumulative pore volumes of all the cement pastes with 0.5 water to cement ratio is always greater than those of the cement pastes with 0.3 water to cement ratio. Hence, either an increase of chloride ions or a reduction of water to cement ratio decreases the cumulative pore volumes of a cement paste.

It was seen from Fig.6 (b) that the most probable pore of specimen without chloride ion is 95.34 nm, and that of specimen with 1% chloride ion is 77.07 nm. It could also be seen from Fig.7(b) that the probable pore size of specimens without chloride ion is 678.47 nm while that of ones with 1% chloride is only 21.09 nm. Hence chloride ions refine the porous structures of hardened paste.

The above observation is well supported by the measured data summarized in the table 2. For the same water to

cement ratio of 0.3, the total intrusion volume and median pore diameter of the cement paste with 1.0 chloride ions are 0.09 (ml/g) and 77.10(nm), which are much smaller than those of 0.14 (ml/g) and 124.81 (nm) of the cement paste without chloride ions. In other words, an increase of chloride ion does refine the pores of a cement paste. However, Table 2 also shows that an increase of chloride ions increases the total pore area of both cement paste with the water to cement ratios of 0.3 to 0.5 from 6.75 to 10.59 m^2/g and from 12.85 to 20.37 m^2/g, respectively. Hence, an increase of chloride ions in a cement paste does refine its porous characteristic, mitigate its carbonation rate and eventually improve durability of a concrete structure.

In order to better exhibit the effect of chloride ion on porous refinement of a cement stone, the three dimensional reconstructed images of the porous structures of two cement pastes, one without chloride and another with 1.0% chloride ion were developed using VG Studio Max 2.1 software and 3D defects analyzing module, as shown in Fig.8.

In Fig.8, the change of the color from blue to red indicates a gradual increase of the pore volume and tiny cracks. It was seen in Fig.8 that chloride ion indeed refines the early porous structures of cement paste and lowers its porosity, which is consistent with what has been observed from Fig. 6, Fig 7 and Table 2.

4. Conclusions

(1) Carbonation rate of a cement paste increases with its carbonation ages and its water to cement ratio, but decreases with its chloride ions content.

(2) Chloride ion of a cement paste refines its porous structures, decreases its porosity and eventually mitigates its carbonation rate.

(3) The X-CT technology can be used to display the progressed carbonation front and the corresponding microstructure evolution of cement paste with its measured data agreed well with those using conventional phenolphthalein method.

Acknowledgements

The authors highly appreciate the financial support from the National Natural Science Foundation of China (5133080, 51308308, 51478227), the project supported by the Major Science and Technology Project of Ningbo(2013C51006), the disciplinary project of Ningbo University (XKL14D2068) and the project supported by K.C Wong Magna Fund in Ningbo University.

References

[1] Zitrou E, Nikoalou J, Tsakiridis PE. Atmospheric corrosion of steel reinforcing bars produced by various manufacturing process. Constr Build Mater 2007; 21 (6):1161–1169.

[2] Pedro FM, Carlos C. Carbonation service life modelling of RC structures for concrete with Portland and blended cements. Cement Concrete Comp 2013; 37(6):171–184.

[3] Du Y G, Clark L A and Chan A H C (2007), Impact of reinforcement corrosion on ductile behavior of reinforced concrete beams, ACI Structural Journal, Vol.104, No. 3, pp 285-293.

[4] Haque MN, Kawamura M. Carbonation and chloride-induced corrosion of reinforcement in fly ash concretes. ACI Mater J 1992; 89(6):602–605.

[5] Song XB, Kong QM, Liu XL. Experimental study on chloride threshold levels in OPC. China Civil Eng J 2007; 40(11):59–63 (in Chinese)

[6] Song HW, Lee CH, Ann KY. Factors influencing chloride transport in concrete structures exposed to marine environments. Ceme Concr Comp 2008; 30(2): 113–121.

[7] Castellote M, Andrade C, Turrillas X et al. Accelerated carbonation of cement pastes in situ monitored by neutron diffraction. Cem Concr Res 2008; 38(2): 1365–1373.

[8] Yang T, Keller B, Magrari E. Dirtect observation of the carbonation process on the surface of calcium hydroxide crystals in hardened cement paste using an atomic force microscope. J Mater Sci 2003; 38:1909–1916.

[9] Suryavanshi AK, Narayan Swamy R. Stability of Friedel's salt in carbonated concrete structural elements. Cem Concr Res 1996; 26(5):729–741.

[10] Kwon S J, Song HW. Analysis of carbonation behavior in concrete using neural network algorithm and carbonation modeling. Cem Concr Res 2010; 40(1): 119–127.

[11] Younsi A, Turcry P, Roziere E et al. Performance-based design and carbonation of concrete with high fly ash content. Cem and Concr comp 2011; 33(2):993 – 1000.

[12] Torgal FP, Miraldo S, Labrincha JA et al. An overview on concrete carbonation in the context of eco-efficient construction: Evaluation, use of SCMs and/or RAC. Constr Build Mater 2012; 36 (4) :141-150.

[13] Meira GR, Andrade C, Vilar EO, Nery K.D. Analysis of chloride threshold from laboratory and field experiments in marine atmosphere zone. Constr Build Mater 2014; 55(31):289-298.

[14] Ramezanianpour AA, Ghahari SA, Esmaeili M. Effect of combined carbonation and chloride ion ingress by an accelerated test method on microscopic and mechanical properties of concrete. Constr Build Mater 2014, 58(15):138-146.

[15] B. Reddy, G.K. Glass, P.J. Lim, N.R. Buenfeld. On the corrosion risk presented by chloride bound in concrete[J]. J Cem Concr Compos, 2002, 24():1–5.

[16] J. Tritthart. Chloride binding in cement II. The influence of the hydroxide concentration in the pore solution of hardened cement paste on chloride binding[J]. Cem Concr Res, 1989,19 :683–691.

[17] I.S. Yoon. Deterioration of concrete due to combined reaction of carbonation and chloride penetration: experimental study. Trans Tech Pub, 2007, 348–349:729–732.

[18] Kuosa H, Ferreira RM, Holt E, et al. Effect of coupled deterioration by freeze-thaw, carbonation and chlorides on concrete service life. Cem and Concr Comp, 2014, 47:32-40.

[19] Sugirama T, Promentilla MAB, Hitomi T, et al. Application of synchrotron microtomography for pore structure characterization of deteriorated cementitious materials due to leaching. Cem Concr Res., 2010; 40(8):1265–1270.

[20] Liu JZ, Xing F, He ZM, et al. Study on critical molar ratios of nitrite and chloride in reinforced Concrete[J]. J Chin Ceram Soc 2004; 32 (7):854–857 (in Chinese)

[21] Song HW, Kwon SJ. Permeability characteristics of carbonated concrete considering capillary pore structure[J]. Cem Concr Res 2007; 37(6): 909–915.

[22] Vilain G, Thiery M, Platret G. Measurement methods of carbonation profiles in concrete: Themogravimetry, chemical analysis and gammadensimetry [J], Cem Concr Res., 2007,37(8):1182-1192.

[23] Hobbes DW. Carbonation of Concrete Containing PFA [J], Magz Concr Res,. 1994,46(166):35-38.

[24] Lu S, Landis EN, Keane DT. X-ray microtomographic studies of pore structure and permeability in portland cement concrete. Mater Struct 2006; 39(6): 611–620.

[25] Rougelot T, Burlion N, Bernard D, et al. About microcracking due to leaching in cementitious composites: X-ray microtomography description and numerical approach. Cem Concr Res 2010; 40(2): 271–283.

[26] Han JD, Pan GH, Sun W. Investigation on carbonation induced meso-defects changes of cement mortar using 3D X-Ray computed tomography [J]. J Chin Ceram Soc, 2011, 399(10):75–79.

[27] Han, JD., Sun W., Pan GH, et al. Monitoring the Evolution of Accelerated Carbonation of Hardened Cement Pastes by X-Ray Computed Tomography[J]. J. Mater. Civ. Eng., 2013,25:347-354.

[28] Han JD., Sun W., Pan GH. X-ray microtomography of the carbonation front shape evolution of cement mortar and modeling of accelerated carbonation reaction[J]. J Wuhan Univ of Techno-Mater. Sci. Ed. 2013,28 (2): 303-308.

[29] Zhou JK, Pan Y, Chen XD. Research advances in Mercury porosimetry study of pore structure in cement-based materials [J]. Material Review 2013, 27(7):72-75.

0 天

Captions of Tables

Table 1 Measured carbonation depth (mm) of specimen using Phenolphthalein

Table 2 Parameters of porous structure of cement paste measured by MIP

Table 1 Measured carbonation depth (mm) of specimen using Phenolphthalein

W/C	Chloride ion /%	Carbonation ages			
		7 (days)	14 (days)	21 (days)	28 (days)
0.3	0	3.4	6.0	6.6	7.1
	0.3	3.1	4.9	6.0	6.4
	0.6	2.2	4.8	5.1	5.7
	1.0	1.9	3.0	4.2	4.8
0.4	0	7.2	9.6	10.3	10.6
	0.3	4.8	7.0	9.1	9.4
	0.6	4.2	6.8	8.0	8.6
	1.0	4.1	5.9	6.9	7.8
0.5	0	9.4	12.5	16.1	17.1
	0.3	8.9	10.8	13.8	14.5
	0.6	6.8	8.8	10.3	11.7
	1.0	6.0	7.3	9.1	10.8

Table 2 Parameters of porous structure of cement paste measured by MIP

W/C	Chloride ion (%)	Total intrusion volume (ml/g)	Total pore area (m^2/g)	Median pore diameter (Volume)/nm	Porosity (%)
0.3	0	0.14	6.75	124.81	24.23
	1	0.09	10.59	77.10	17.69
0.5	0	0.21	12.85	179.72	32.03
	1	0.17	20.37	55.61	26.84

Captions of Figures:

Fig.1. X-CT scanner (a)Set up (b) Principle

Fig.2. X-CT pictures of specimen with 0.3 water-to-cement ratio at different carbonation ages

Fig.3. X-CT picture of specimen with 0.5 water-to-cement ratio at different carbonation ages

Fig.4.3D-gray-values histograms of specimen with 0.5 water-to-cement ratio at different carbonation ages (note: C=Carbonation, NC=Non-carbonation) (a) $[Cl^-]$=0.3% before carbonation ;(b) $[Cl^-]$=0.3% 7-day carbonation age; (c) $[Cl^-]$=0.3% 21-day carbonation age; (d) $[Cl^-]$=1% before carbonation; (e) $[Cl^-]$=1% 7-day carbonation age; (f) $[Cl^-]$=1% 21-day carbonation age

Fig.5. Top view (left) and side view (right) images and line gray values distribution at different carbonation ages (note :P=Pore; X=X-ray beam hardening; C=Carbonation; NC=Non-carbonation) (a) 0 day carbonation; (b) 7-day carbonation age; (c) 21-day carbonation age

(Note: NC-No Carbonation; C-Carbonation; X-X-ray beam hardening; P-Pore)

Fig.6. Porous structures of specimen with 0.3 water-to-cement ratio (a) Cumulative pore volumes; (b) Pore size distribution

Fig.7. Porous structures of specimens with 0.5 water-to-cement ratio (a) Cumulative pore volumes; (b) Pore size distribution

Fig.8. Porous structures of cement paste with water cement ratio of 0.5 by X-CT

Captions of Figures:

Fig.1. X-CT scanner (a)Set up (b) Principle

Fig.2. X-CT pictures of specimen with 0.3 water-to-cement ratio at different carbonation ages

Fig.3. X-CT picture of specimen with 0.5 water-to-cement ratio at different carbonation ages

Fig.4.3D-gray-values histograms of specimen with 0.5 water-to-cement ratio at different carbonation ages (note: C=Carbonation, NC=Non-carbonation) (a) $[Cl^-]$=0.3% before carbonation ;(b) $[Cl^-]$=0.3% 7-day carbonation age; (c) $[Cl^-]$=0.3% 21-day carbonation age; (d) $[Cl^-]$=1% before carbonation; (e) $[Cl^-]$=1% 7-day carbonation age; (f) $[Cl^-]$=1% 21-day carbonation age

Fig.5. Top view (left) and side view (right) images and line gray values distribution at different carbonation ages (note :P=Pore; X=X-ray beam hardening; C=Carbonation; NC=Non-carbonation) (a) 0 day carbonation; (b) 7-day carbonation age; (c) 21-day carbonation age

(Note: NC-No Carbonation; C-Carbonation; X-X-ray beam hardening; P-Pore)

Fig.6. Porous structures of specimen with 0.3 water-to-cement ratio (a) Cumulative pore volumes; (b) Pore size distribution

Fig.7. Porous structures of specimens with 0.5 water-to-cement ratio (a) Cumulative pore volumes; (b) Pore size distribution

Fig.8. Porous structures of cement paste with water cement ratio of 0.5 by X-CT

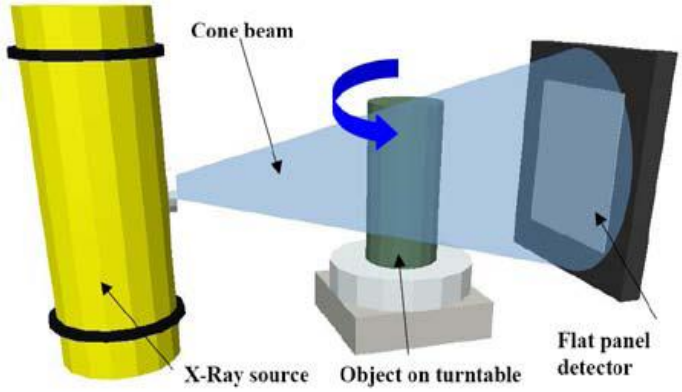

(a) Set up

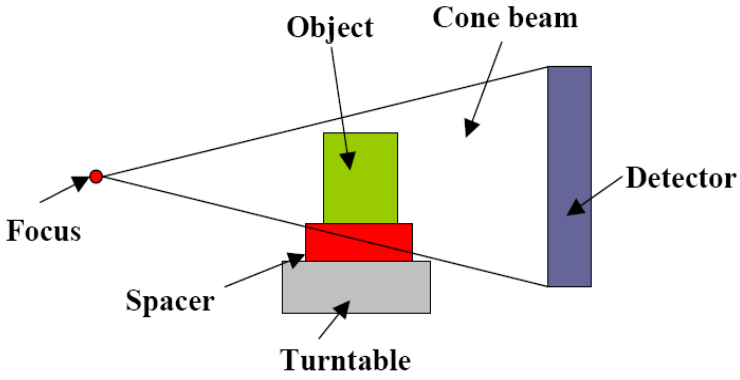

(b) Principle

Fig.1 X-CT measurement with flat panel detector [27]

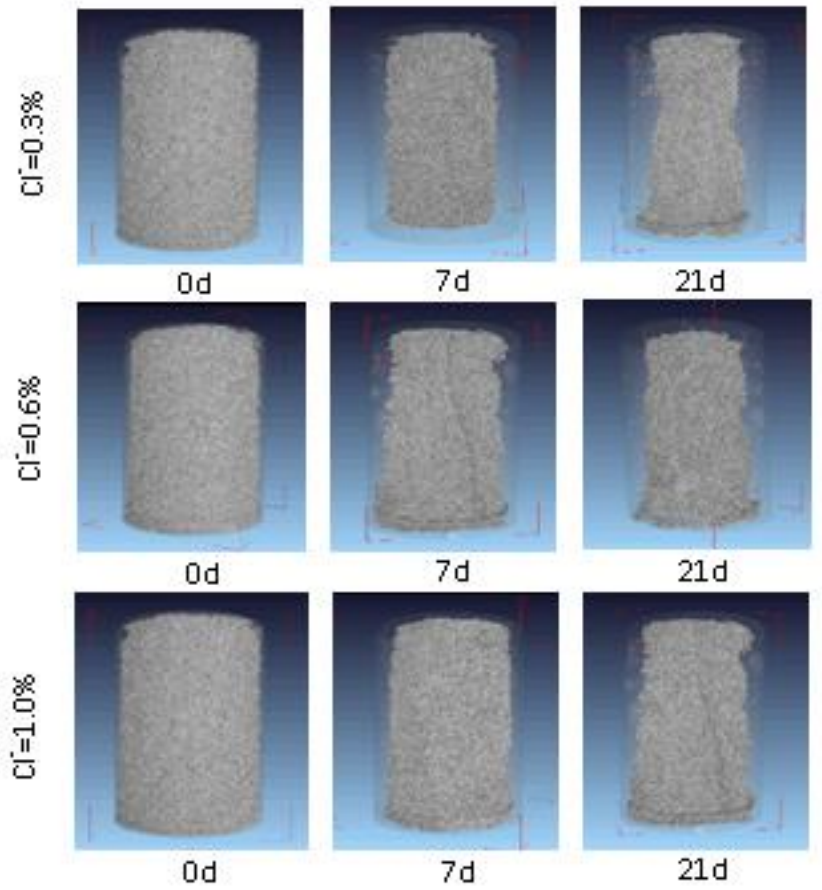

Fig.2. X-CT images of the cement cylinder with water to cement ratio of 0.3 at different carbonation ages

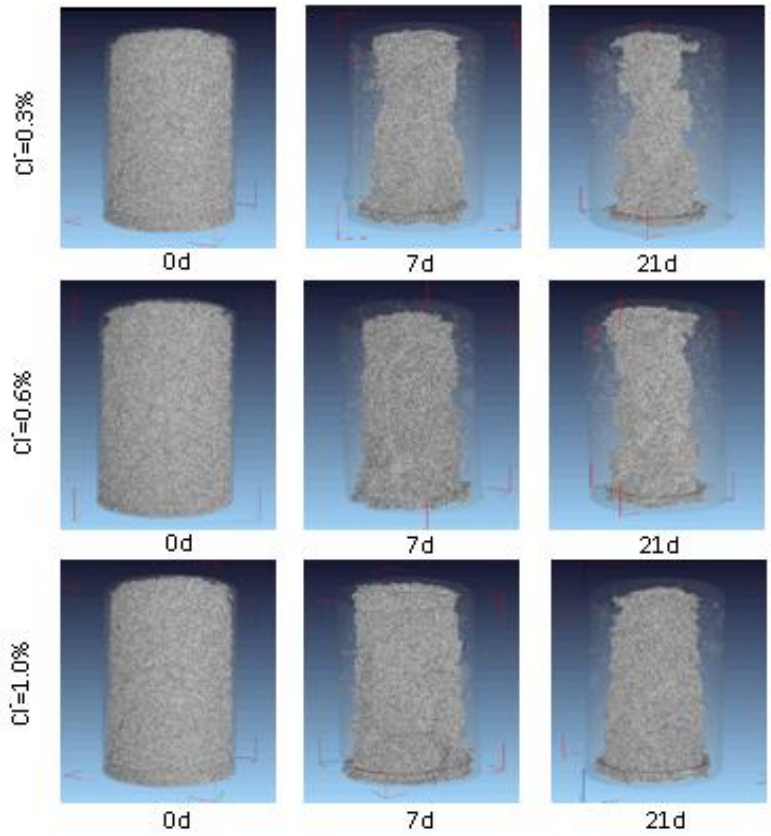

Fig.3. X-CT images of the cement cylinder with water to cement ratio of 0.5 at different carbonation ages

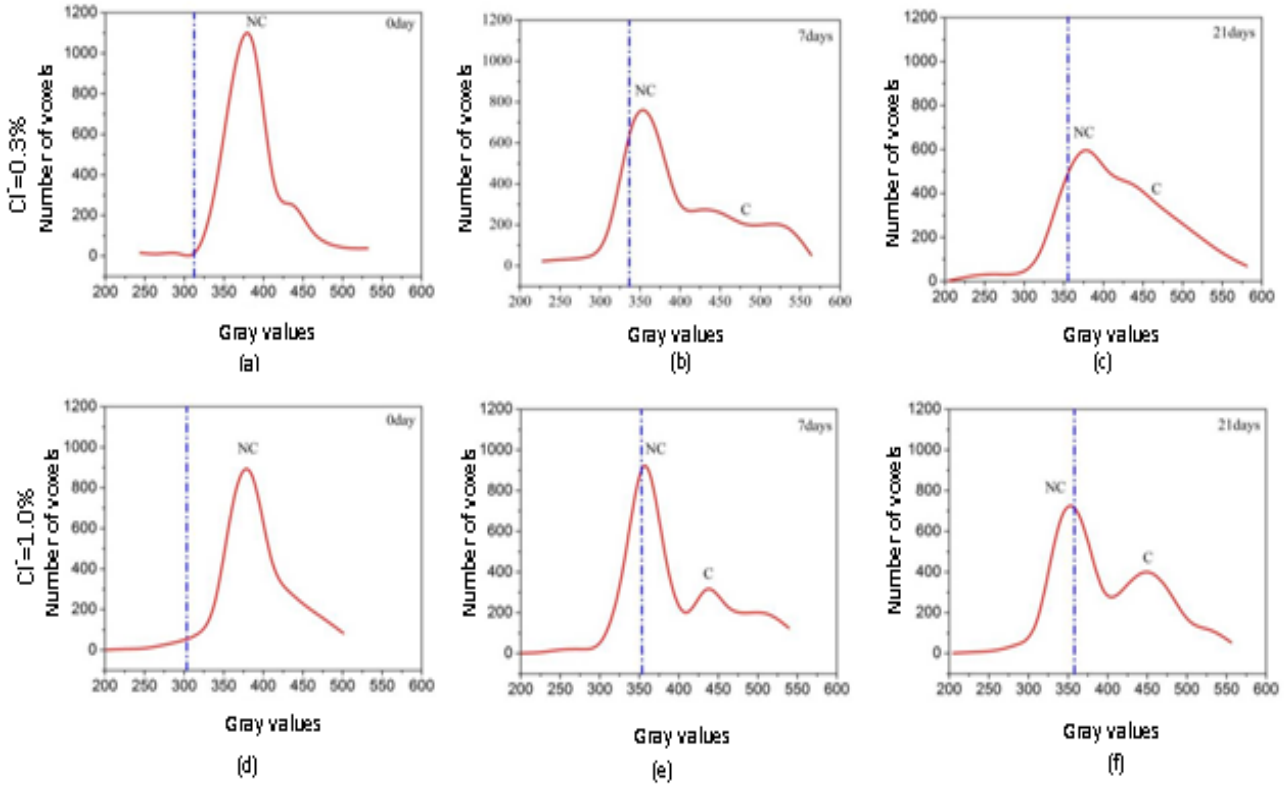

Fig.4. 3D gray values histograms with different carbonation ages (note: C=Carbonation, NC=Non-carbonation)

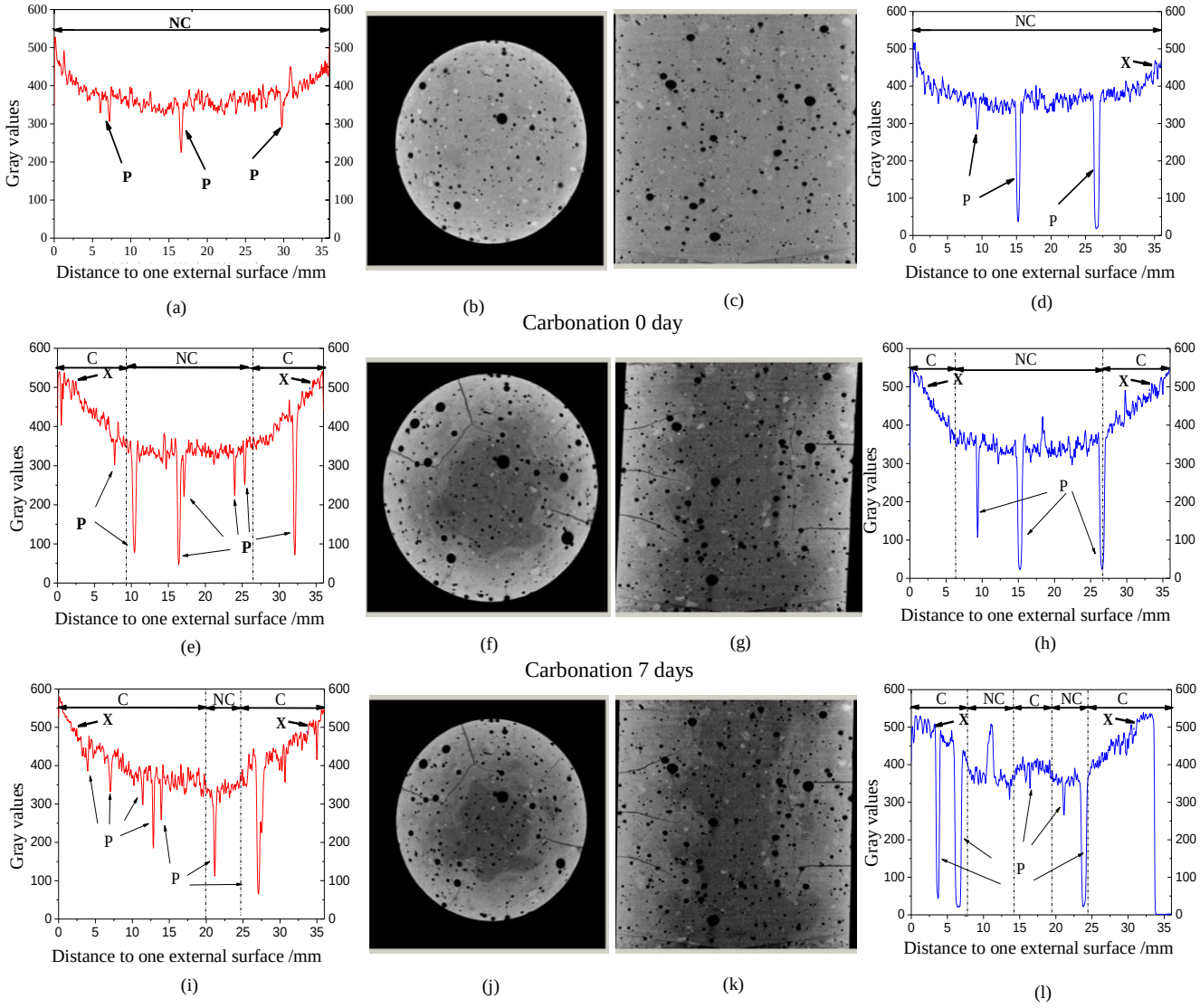

Fig.5 Top view (left) and side view (right) images and line gray values distribution of different carbonation ages (note :P=Pore; X=X-ray beam hardening; C=Carbonation; NC=Non-carbonation)

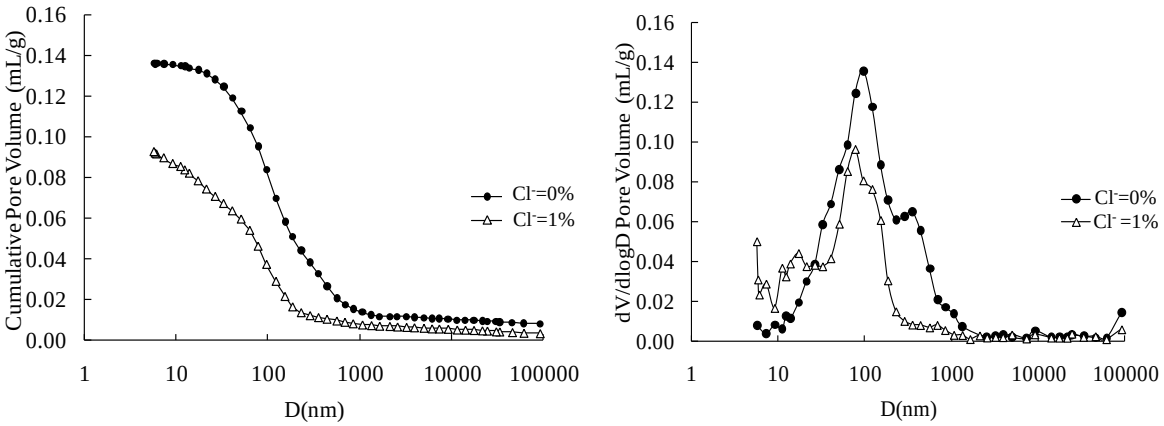

(a) Accumulating porosity (b) Pore distribution

Fig.6 Porous structures of specimen with 0.3 water-to-cement ratio

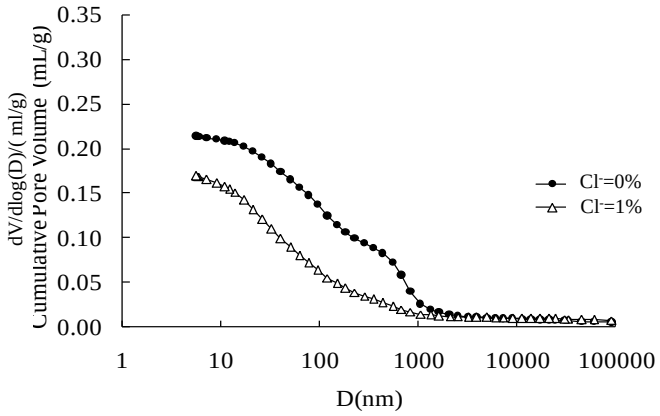

438

439

440

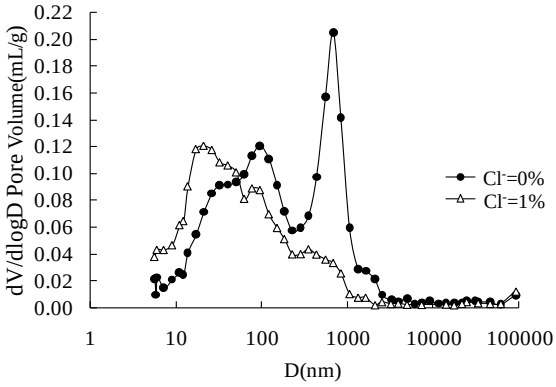

441 Fig.7

442 (a) Accumulating porosity (b) Pore distribution

443 Fig.7. Porous structures of specimens with 0.5 water-to-cement ratio

444

445

446

447

448

449

450

451

452

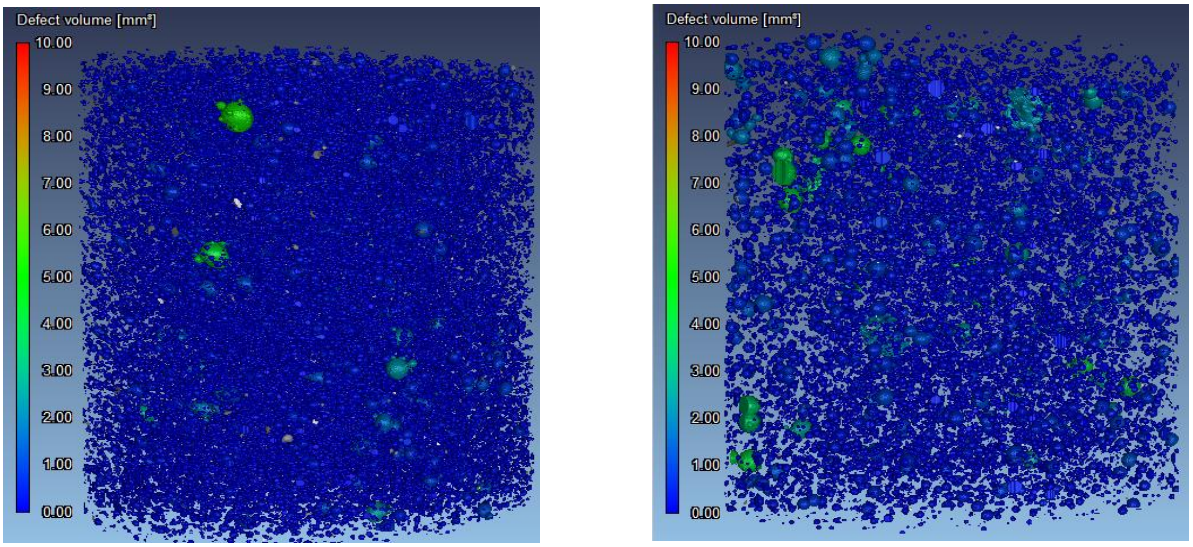

(a) Cl^-=0% (b) Cl^-=1%

Fig.8 Porous structures of cement paste with water cement ratio of 0.5 by X-CT

453

454

455

456

457

458

459

460

461

462

463

464

465

466

467